



Depiction of Aging-Based Molecular Phenotypes With Diverse Clinical Prognosis and Immunological Features in Gastric Cancer

Fang He^{1†}, Huan Ding^{1†}, Yang Zhou², Yuanzhen Wang¹, Juan Xie¹, Shaoqi Yang^{1*} and Yongzhao Zhu^{1*}

¹ General Hospital of Ningxia Medical University, Yinchuan, China, ² Graduate School, Ningxia Medical University, Yinchuan, China

OPEN ACCESS

Edited by:

Fu Wang,
Xi'an Jiaotong University, China

Reviewed by:

Francesca Reggiani,
Local Health Authority of Reggio
Emilia, Italy
Weimin Zhong,
Xiamen Fifth Hospital, China

*Correspondence:

Yongzhao Zhu
zhuyongzhao2410@nyfy.com.cn
Shaoqi Yang
shaoqiynh@nyfy.com.cn

[†]These authors have contributed
equally to this work

Specialty section:

This article was submitted to
Precision Medicine,
a section of the journal
Frontiers in Medicine

Received: 11 October 2021

Accepted: 10 November 2021

Published: 01 February 2022

Citation:

He F, Ding H, Zhou Y, Wang Y, Xie J, Yang S and Zhu Y (2022) Depiction of Aging-Based Molecular Phenotypes With Diverse Clinical Prognosis and Immunological Features in Gastric Cancer. *Front. Med.* 8:792740. doi: 10.3389/fmed.2021.792740

Objective: Aging acts as a dominating risk factor for human cancers. Herein, we systematically dissected the features of transcriptional aging-relevant genes in gastric cancer from multiple perspectives.

Methods: Based on the transcriptome profiling of prognostic aging-relevant genes, patients with gastric cancer in The Cancer Genome Atlas (TCGA) stomach adenocarcinoma (TCGA-STAD) cohort were clustered with a consensus clustering algorithm. Mutational landscape and chemotherapeutic responses were analyzed and immunological features (immunomodulators, immune checkpoint molecules, cancer immunity cycle, and tumor-infiltrating immune cells) were systematically evaluated across gastric cancer. Weighted gene co-expression network (WGCNA) was conducted for screening aging molecular phenotype-relevant genes, and key genes were identified with Molecular Complex Detection (MCODE) analyses. Expressions of key genes were examined in 20 paired tumors and controls with RT-qPCR and Western blotting. Proliferation and apoptosis were investigated in two gastric cancer cells under MYL9 deficiency.

Results: Three aging-based molecular phenotypes (namely, C1, C2, and C3) were conducted in gastric cancer. Phenotype C1 presented the most prominent survival advantage and highest mutational frequencies. Phenotype C2 indicated low responses to sorafenib and gefitinib, while C3 indicated low responses to vinorelbine and gemcitabine. Additionally, phenotype C2 was characterized by enhanced immune and stromal activation and an inflamed tumor microenvironment. Seven aging molecular phenotype-relevant key genes (ACTA2, CALD1, LMOD1, MYH11, MYL9, MYLK, and TAGLN) were identified, which were specifically upregulated in tumors and in relation to dismal prognosis. Among them, MYL9 deficiency reduced proliferation and enhanced apoptosis in gastric cancer cells.

Conclusion: Collectively, aging-based molecular subtypes may offer more individualized therapy recommendations and prognosis assessment for patients in distinct subtypes.

Keywords: gastric cancer, aging-relevant genes, molecular phenotype, prognosis, tumor immune microenvironment, immunogenomic characteristics

INTRODUCTION

Gastric cancer ranks the sixth most frequent malignancy as well as the fifth major cause of cancer death across the globe (1). When diagnosed at an advanced stage, patients' 5-year overall survival rate is merely 5% (1). As a heterogeneous disease, it has the features of diverse histological and molecular subtypes (2). At present, according to the morphology, differentiation, and cohesion of gland cells, gastric cancer is histopathologically classified as intestinal and diffuse (3). Genomic analyses have become the major methodology applied in international efforts for discovering novel biological targets in gastric cancer (4). It is fundamental to unravel the complicated biology underlying gastric cancer etiology and development for overcoming the highly heterogeneous malignancy.

Accumulated pieces of evidence have uncovered the implication of tumor-associated structures and activated signaling pathways both in tumor cells and in the tumor microenvironment (5). Aging is a complicated process primarily categorized by a reduction in tissues, cells, and organ functions as well as an elevated risk of mortality, which acts as a dominant risk factor of diverse fatal malignancies, especially cancers (6). This process presents prominent correlations to telomere attrition, mitochondrial dysfunction, DNA injury, impaired immune system, and the like (7). Nevertheless, the specific mechanisms involved in aging are still indistinct. Transcriptomic studies have identified abundant human aging-relevant genes (8). The human aging genome resource (HAGR) project offers a powerful set of aging-specific network features, which reveals aging-relevant gene signatures as network hubs through comprehensive analyses of biology and genetics of the human aging process (8). Cellular senescence is a permanent state of stagnant replication of proliferating cells as well as a sign of aging (9). Senescent tumor cells triggered by tumorigenesis may lead to cell cycle arrest, as an antitumor mechanism (10). Nevertheless, senescent cells surrounding tumor cells generate opposite results as well as present prominent correlations with senescence-associated secretory phenotype factor secretions (11). Moreover, senescence displays two-tier influences upon cancer immunity (12, 13). Aging-relevant gene signatures exert critical functions in modulating cellular senescence, not only inhibiting tumor progression through modulating senescence of cancer cells but also promoting malignant progression of cancers and dismal clinical outcomes (14). Nevertheless, there is still a lack of systematic analyses of aging-relevant genes during

gastric carcinogenesis. Herein, we identified three aging-based molecular phenotypes that offered more individualized therapy options and prognosis prediction for gastric cancer patients.

MATERIALS AND METHODS

Retrieval and Preprocessing of Genome-Relevant Data and Clinical Information

Raw RNA-seq data [Fragments Per Kilobase Million (FPKM) value] and relevant clinicopathological characteristics for The Cancer Genome Atlas (TCGA) stomach adenocarcinoma (TCGA-STAD) cohort containing 443 patients with gastric cancer were curated from Genomic Data Commons (GDC) data portal (<https://portal.gdc.cancer.gov>) utilizing TCGAbiolinks package (15). Additionally, normalized microarray expression profiling of 433 patients with gastric cancer in the GSE84437 cohort was curated from the Gene Expression Omnibus (GEO) repository (<https://www.ncbi.nlm.nih.gov/gds/>) (16). The detailed information of patients with gastric cancer in TCGA and GSE84437 cohorts is listed in **Supplementary Table 1**. The expression profiling (FPKM values) of the TCGA-STAD dataset was transformed into transcripts per kilobase million (TPMs). In total, 307 aging-relevant genes (**Supplementary Table 2**) were curated from the HAGR (<https://genomics.senescence.info/>) (8). Molecular subtypes [genome stable (GS), microsatellite instability (MSI), EBV infection, and chromosomal instability (CIN)] of gastric cancer samples were retrieved from Liu et al. (17). Somatic mutation data [Mutation Annotation Format (MAF) format] of 433 patients with gastric cancer on the basis of the whole-exome sequencing platforms were curated from the TCGA project. Mutational types and frequencies of genes were analyzed as well as visualized utilizing the maftools package (18). Tumor mutation burden (TMB) was defined as the entire number of non-synonymous variations within the coding regions per megabase (19). In addition, copy number alteration (CNA) data were retrieved from GDAC Firehose (<https://gdac.broadinstitute.org>), and prominent amplification and deletion across the whole genome were identified with GISTIC2.0 (20). Somatic copy-number alterations (SCNAs) and homologous recombination deficiency (HRD) across gastric cancer specimens were also curated from Davoli et al. (21).

Molecular Characterization for Subtypes

Tumors with qualitatively diverse aging-relevant gene expressions were clustered utilizing hierarchical agglomerative clustering on the basis of Euclidean distance as well as Ward's linkage. Unsupervised clustering method (K-means) was utilized for identifying aging-related molecular phenotypes as well as classifying samples for subsequent analyses. Through consensus clustering algorithm, the number of clusters was determined using TCGA-STAD and GSE84437 cohorts for assessing the stability of the identified molecular phenotypes. This procedure was presented through adopting the ConsensusClusterPlus package as well as repeated 50 times for ensuring the accuracy regarding this classification (22).

Abbreviations: FPKM, Fragments Per Kilobase Million; TCGA, The Cancer Genome Atlas; GDC, Genomic Data Commons; GEO, Gene Expression Omnibus; TPMs, transcripts per kilobase million; TMB, Tumor mutation burden; can, copy number alteration; SCNAs, Somatic copy-number alterations; PCA, Principal component analyses; GSA, gene set variation analysis; MSigDB, Molecular Signatures Database; Pan-F-TBRS, pan-fibroblast TGF- β response signature; EMT, epithelial-mesenchymal transition; ssGSEA, single sample gene set enrichment analysis; GDSC, Genomics of Drug Sensitivity in Cancer; IC50, half-maximal inhibitory concentration; ESTIMATE, Estimation of Stromal and Immune cells in Malignant Tumor tissues using Expression data; WGCNA, Weighted gene co-expression network analysis; STRING, Search Tool for the Retrieval of Interacting Genes/Proteins; PPI, protein-protein interaction; MCODE, Molecular Complex Detection; RT-qPCR, Real-time quantitative reverse transcription PCR.

Gene Set Variation Analysis (GSVA)

Gene set variation analysis, a non-parametric and unsupervised gene set enrichment algorithm, may infer the enrichment scores of specific pathways or signatures on the basis of transcriptomic profiling (23). The 50 hallmarks of gene signatures were collected from the Molecular Signatures Database (MSigDB) project (24). Moreover, the gene sets of other relevant biological processes were curated from Mariathasan et al. containing CD8 T effectors, DNA damage repair, pan-fibroblast TGF- β response signature (Pan-F-TBRS), antigen-processing machinery, immune checkpoint, epithelial-mesenchymal transition (EMT) markers, FGFR3-related genes, angiogenesis, Fanconi anemia, WNT targets, cell cycle regulators, and the like (25). Utilizing single sample gene set enrichment analysis (ssGSEA) from the GSVA package, gene sets of hallmarks and other relevant biological processes were chosen for presenting quantifications of pathway activity.

Estimation of Chemotherapeutic Response

Chemotherapeutic sensitivity in cancer cells, as well as molecular markers of chemotherapeutic response profiles, were curated from the largest publicly available pharmacogenomics project: the Genomics of Drug Sensitivity in Cancer (GDSC; <https://www.cancerrxgene.org/>) (26). Four commonly applied chemotherapeutic agents, sorafenib, gefitinib, vinorelbine, and gemcitabine, were chosen. The prediction procedure was implemented *via the* pRRophetic package (27). The half-maximal inhibitory concentration (IC₅₀) values were estimated with the ridge regression method, and the prediction accuracy was assessed through 10-fold cross-verification.

Evaluation of Tumor Immune Microenvironment and Immunogenomic Characteristics

Immunological features of the tumor immune microenvironment contained the expression profiles of immunomodulatory factors and immune checkpoint molecules, the activity of the cancer immunity cycle, and infiltrations of immune cells. In total, 122 immunomodulatory factors comprising MHC, receptor, chemokine, and immune stimulator were curated from Sokolov et al. (28). Immune checkpoint molecules with therapeutic potential were collected from Auslander et al. (29). The cancer immunity cycle uncovers antitumor immune response, and the activity of each step determines the fate of tumor cells (30). Here, the activity of each step was quantified with ssGSEA on the basis of the expression profiling of individual specimens. Thereafter, the ssGSEA algorithm was developed for quantifying the abundance of lymphocytes within the tumor immune microenvironment utilizing bulk RNA-seq profiles. Through Estimation of Stromal and Immune cells in Malignant Tumor tissues using Expression data (ESTIMATE), immune and stromal contents (immune and stromal scores and tumor purity) were inferred across gastric cancer specimens (31). Tumor tissues with abundant immune cell infiltration represented an increased immune score and a decreased level of tumor purity.

Quantification of Gene Expression-Based Stemness Index (MRNasi)

Through the one-class logistic regression (OCLR) method, the stemness index was calculated on the basis of transcriptome profiling of normal PSCs (32). The stemness signatures were generated with the OCLR algorithm (28). Thereafter, this study estimated Spearman's correlation between the weight vector of the stemness signatures and mRNA expression across gastric cancer. Eventually, the stemness index was mapped onto the range of 0 to 1 utilizing a linear conversion, which subtracted the minimum as well as separated through the maximal correlation coefficient. The stemness index produced from transcriptome profiling was defined as mRNasi.

Weighted Gene Co-expression Network Analysis (WGCNA)

Weighted gene co-expression network analysis was presented for identifying underlying co-expression modules that were prominently correlated with aging-associated molecular phenotypes. The soft-thresholding for the scale-free network was identified. The topological overlap matrix similarity was adopted for the evaluation of the distance between gene pairs. Furthermore, hierarchical clustering analyses with mean and dynamic methods were utilized for building the clustering tree as well as classifying the gene signatures into diverse modules. Following merging the initial modules in line with their similarity, functional modules were eventually conducted. Spearman's correlation coefficient, as well as matched *p*-value between aging-associated molecular phenotypes and functional modules, was determined through *cor* function. For each module, gene significance (GS) and module membership (MM) were calculated. Genes with $GS > 0.5$ and $MM > 0.8$ were utilized as aging phenotype-relevant genes. Through the Search Tool for the Retrieval of Interacting Genes/Proteins (STRING) tool (33), protein-protein interaction (PPI) analysis of aging phenotype-relevant genes was carried out. Molecular Complex Detection (MCODE) (34), a plugin in Cytoscape software (35), was used for screening the significant modules of the PPI network in line with the filtering criteria of degree cutoff = 2, node score cutoff = 0.2, k-core = 2, and depth from depth = 100.

Patients and Specimens

In total, 20 patients with gastric cancer were recruited at the General Hospital of Ningxia Medical University. Adjacent gastric tissues (3–6 cm from the tumor). Tumor tissues and adjacent non-cancerous gastric tissues (>5 cm from the edge of tumor tissues) were harvested during surgical resection. The inclusion criteria included: (1) patients pathologically diagnosed with gastric cancer and (2) patients who did not experience radio- and/or adjuvant chemotherapy prior to surgery. The exclusion criteria included: (1) patients previously diagnosed with other malignancies; (2) patients who were previously treated with radio- or adjuvant chemotherapy; and (3) patients who died within 4 weeks of this surgery. All specimens were frozen in liquid nitrogen at once following collection and were stored at -80°C before usage. This study was conducted in accordance with the

TABLE 1 | Primer sequences used for RT-qPCR.

Gene	Sequence (5'-3')
MYL9	F: TCTTCGCAATGTTTGACCAGT R: GTTGAAAGCCTCCTTAACTCCT
ACTA2	F: AAAAGACAGCTACGTGGGTGA R: GCCATGTTCTATCGGGTACTTC
TAGLN	F: AGTGCAGTCCAAAATCGAGAAG R: CTTGCTCAGAATCACGCCAT
MYH11	F: CGCCAAGAGACTCGTCTGG R: TCTTTCCCAACCGTGACCTTC
LMOD1	F: GTAAAAGGGGAGCGTAGGAAC R: CTCGGGTGTTTTGGTCTTGCT
CALD1	F: TGGAGGTGAATGCCAGAAC R: GAAGGCGTTTTGGCGTCTTT
MYLK	F: CCCGAGTTGTCTGGTTCAAA R: GCAGGTGTACTTGGCATCGT
GAPDH	F: CTGGGCTACACTGAGCACC R: AAGTGGTCGTTGAGGGCAATG

guidance of the Declaration of Helsinki. The protocol gained the approval of the Institutional Ethical Committee of General Hospital of Ningxia Medical University (Approval No. 2020-031). All participants signed an informed consent form prior to our study.

Real-Time Quantitative Reverse Transcription PCR

Tissues or cells were lysed with RNAiso plus (Takara, Japan). Thereafter, RNA extraction was presented with the phenol-chloroform/isopropanol method. The cDNA was prepared through PrimeScript RT reagent kits as well as a gDNA eraser. About 20 μ l qPCR system was prepared, followed by analysis with GoTaq qPCR Master Mix. The relative mRNA expressions were quantified with the $2^{-\Delta\Delta Ct}$ method, with GAPDH as a control. The primer sequences are listed in **Table 1**.

Western Blotting

Tissues or cells were lysed with RIPA buffer plus protease inhibitor cocktail. Following separation *via* electrophoresis in SDS/PAGE gel, the protein was transferred onto PVDF membranes. The membrane was blocked in PBS-T buffer in supplements of 5% milk/BSA lasting 2 h and presented the incubation with primary antibody targeting MYL9 (1:500; 15354-1-AP; Proteintech, China), ACTA2 (1:1000; 23081-1-AP; Proteintech, China), TAGLN (1:300; 15502-1-AP; Proteintech, China), MYH11 (1:1000; 18569-1-AP; Proteintech, China), LMOD1 (1:500; 15117-1-AP; Proteintech, China), CALD1 (1:2000; 20887-1-AP; Proteintech, China), MYLK (1:500; 21642-1-AP; Proteintech, China), and β -actin (1:5000; 20536-1-AP; Proteintech, China) overnight at 4°C. Following incubation by horseradish peroxidase-labeled HRP-coupled secondary antibodies lasting 1 h, the protein band was visualized with an ECL detection reagent.

Cell Culture

Two gastric cancer cell lines (MGC-803 and BGC-823) were acquired from the Cell Bank of the Chinese Academy of Sciences (Shanghai, China). The cells were cultivated in the Dulbecco's modified Eagle's medium (DMEM; Gibco, United States) with supplements of 10% fetal bovine serum (FBS) as well as 1% antibiotics penicillin/streptomycin. Moreover, all cells were fostered in an incubator with 5% CO₂ at 37°C.

Transfection

For generating MYL9-knockdown clones, two short hairpin RNA (shRNA) sequences against MYL9 were synthesized and cloned into pSUPER-retro-puro plasmids. The recombinant plasmids or negative control vector ligated by scrambled-base hairpin oligos were co-transfected with packaging plasmids pIK into 293T cells. Thereafter, the supernatant was harvested, which was utilized for infecting MGC-803 and BGC-823 cells. The above-mentioned cells were plated into 6-well plates. When the confluency reached 50%, transfections were presented with Lipofectamine 2000 (Invitrogen, United States) in accordance with the manufacturer's instructions. Following 48 h, transfection efficiencies were evaluated.

Cell Counting Kit (CCK)-8

For the determination of viable MGC-803 and BGC-823 cells, CCK-8 (Dojindo, Japan) kits were adopted. In brief, cells were administered on a 96-well plate (3×10^3 cells/well). Following cultivation lasting 24 h, 10 μ l of CCK-8 reagent was added, followed by incubation at 37°C lasting 1 h. The absorbance values were tested at 450 nm with an ultraviolet spectrophotometer at diverse time points.

Flow Cytometry

MGC-803 and BGC-823 cells were treated with propranolol lasting 24 h. Thereafter, 100 μ l cell suspension was incubated with 5 μ l fluorescein isothiocyanate (FITC)-Annexin V as well as 2.5 μ l propidium iodide (PI) protecting from light in accordance with the manufacturer's instruction. Apoptosis was under evaluation utilizing flow cytometry on BD FACSCanto II (BD, United States). Flow cytometry was analyzed with FlowJo software.

Statistics

All statistical analyses were conducted with R software and GraphPad Prism software. Measurement data were displayed as mean \pm SD. If the variables were normally distributed, comparisons of continuous variables between two or more than two subgroups were presented through a parametric test (Student's *t*-test or ANOVA). Otherwise, a non-parametric test (Wilcoxon rank-sum test or Kruskal-Wallis test) was presented. Principal component analyses (PCAs) were used to present the dissimilarity among diverse clusters. Hazard ratio (HR) was determined with a Cox regression model utilizing a survival package. Analyses of overall survival (OS), disease-free survival (DFS), and disease-specific survival (DSS) were conducted with Kaplan-Meier method, and the log-rank test was adopted for determining the statistical difference. Pearson's or Spearman's

TABLE 2 | Prognostic aging-relevant genes in gastric cancer with univariate-cox regression analyses.

Genes	HR	HR 0.95L	HR 0.95H	P-value
GHR	1.5437	1.1596	2.0551	0.0029
POU1F1	3.5083	1.2136	10.142	0.0205
GH1	1.9524	1.0594	3.5981	0.0320
NGF	1.7419	1.2548	2.4180	0.0009
EGF	1.5420	1.1022	2.1572	0.0115
PDGFRB	2.2543	1.1351	4.4766	0.0202
PEX5	0.3813	0.1479	0.9831	0.0460
NR3C1	2.0259	1.1514	3.5646	0.0143
TGFB1	3.0279	1.2103	7.5751	0.0179
APOC3	1.2600	1.0596	1.4984	0.0089
AR	1.3530	1.0050	1.8215	0.0463
FEN1	0.4273	0.1849	0.9872	0.0466
A2M	2.4406	1.0382	5.7374	0.0408
SNCG	1.7807	1.2627	2.5113	0.0010
PON1	1.4702	1.0866	1.9893	0.0125
IL6	1.3283	1.0257	1.7201	0.0314
FGFR1	1.5856	1.0199	2.4652	0.0406
PAPPA	1.6353	1.1335	2.3593	0.0085
EFEMP1	1.9565	1.2875	2.9732	0.0017
AGTR1	1.2752	1.0316	1.5763	0.0246
PDGFRA	1.8412	1.1501	2.9478	0.0110

correlation test was used for evaluating the correlation between variables. For all statistical analyses, a two-tailed $P < 0.05$ indicated significance.

RESULTS

Aging-Genomic Profiles Identify Three Diverse Molecular Phenotypes of Gastric Cancer

This study analyzed the expression patterns of aging-relevant genes across gastric cancer specimens in the TCGA cohort. Through univariate-cox regression analyses, abnormal expression of 24 aging-relevant genes was in relation to gastric cancer prognosis (Table 2). With the consensus clustering method, patients with gastric cancer were clustered into three aging-relevant molecular phenotypes (C1, 143 samples; C2, 117 samples; C3, 91 samples) in accordance with the transcriptome profiling of prognostic aging-relevant genes (Figure 1A). PCA uncovered the dissimilarity between aging-relevant molecular phenotypes (Figure 1B). The prominent discrepancy in expressions of prognostic aging-relevant genes was investigated among phenotypes (Figure 1C). Survival analyses demonstrated that three aging-relevant molecular phenotypes presented prominent survival outcomes. C1 phenotype possessed more favorable OS (Figure 1D), DFS (Figure 1E), and DSS (Figure 1F) outcomes than C2 and C3 phenotypes. The classification accuracy was confirmed in the GSE84437 cohort (Supplementary Figures 1A–D). Figure 1G

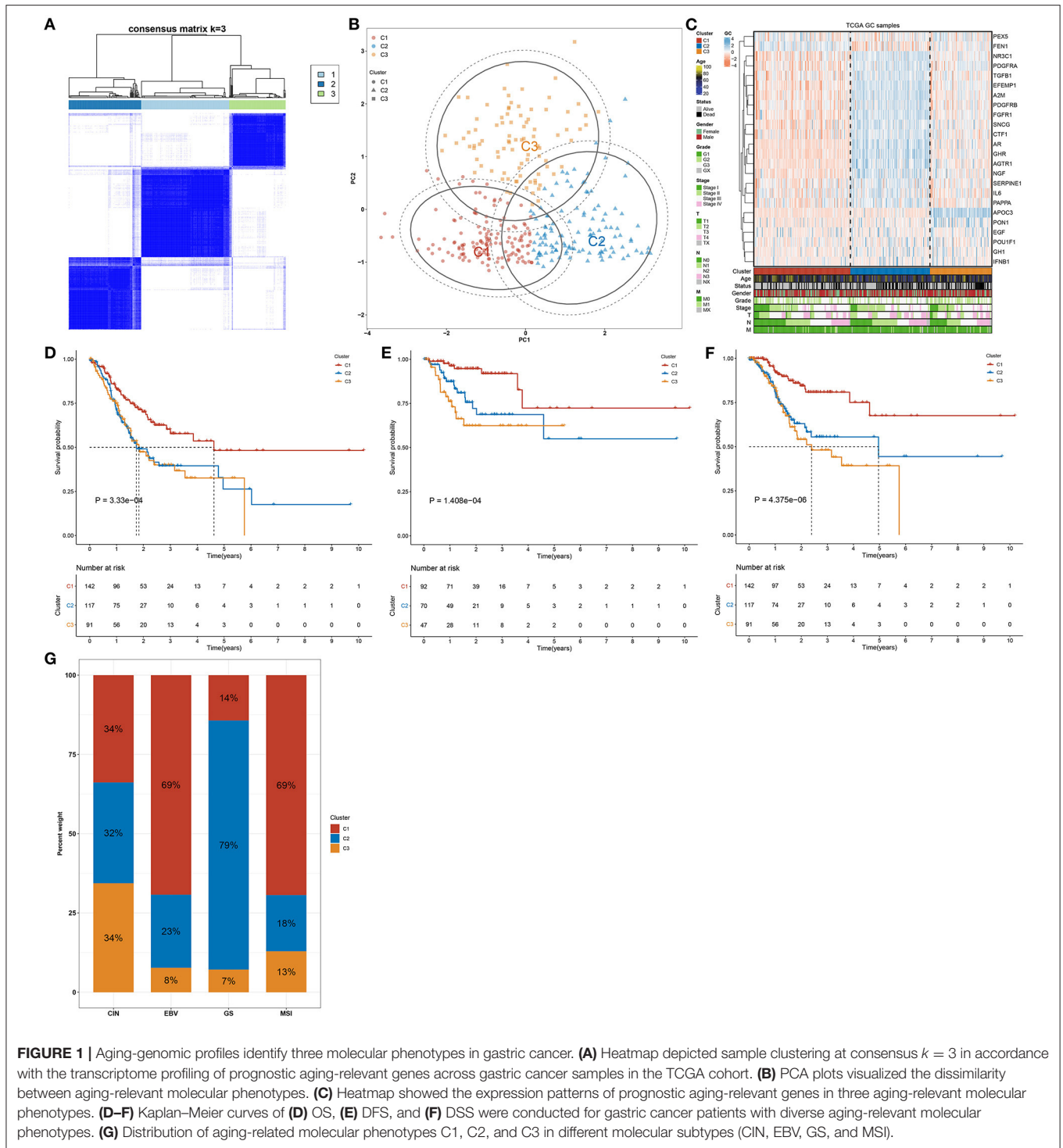
showed the heterogeneity in the distribution of three aging-relevant molecular phenotypes (C1, C2, and C3) among the most known molecular subtypes (CIN, EBV, GS, and MSI). C1 subtype occupied the highest percentage in EBV and MSI, while C2 occupied the highest percentage in GS. Thus, the aging-relevant molecular phenotypes presented remarkable associations with the most known molecular subtypes of gastric cancer.

Aging-Relevant Molecular Phenotypes With Diverse Cancer Mutational Genome

The preclinical studies and clinical trials have uncovered that somatic mutation is linked to therapeutic response, survival outcome, and clinical benefit of patients with gastric cancer (36). Hence, this study evaluated the distributions of somatic mutations across gastric cancer among three aging-related molecular phenotypes. We investigated that molecular phenotype C1 presented higher mutational frequency (132, 30.48%; Figure 2A) compared with C2 (84, 19.4%; Figure 2B) and C3 (86, 19.86%; Figure 2C). The first 20 genes with the highest mutational frequencies were shown in each phenotype. Gistic2.0 identified 54 amplifications in phenotype C1 (Figure 2D), 37 amplifications in phenotype C2 (Figure 2E), and 58 amplifications in phenotype C3 (Figure 2F). Meanwhile, there were 46 deletions in phenotype C1 (Figure 2G), 35 deletions in phenotype C2 (Figure 2H), and 51 deletions in phenotype C3 (Figure 2I). Collectively, aging-relevant molecular phenotypes presented diverse cancer mutational genomes.

Aging-Associated Molecular Phenotypes With Distinct Activations of Functional Pathways and Chemotherapeutic Responses

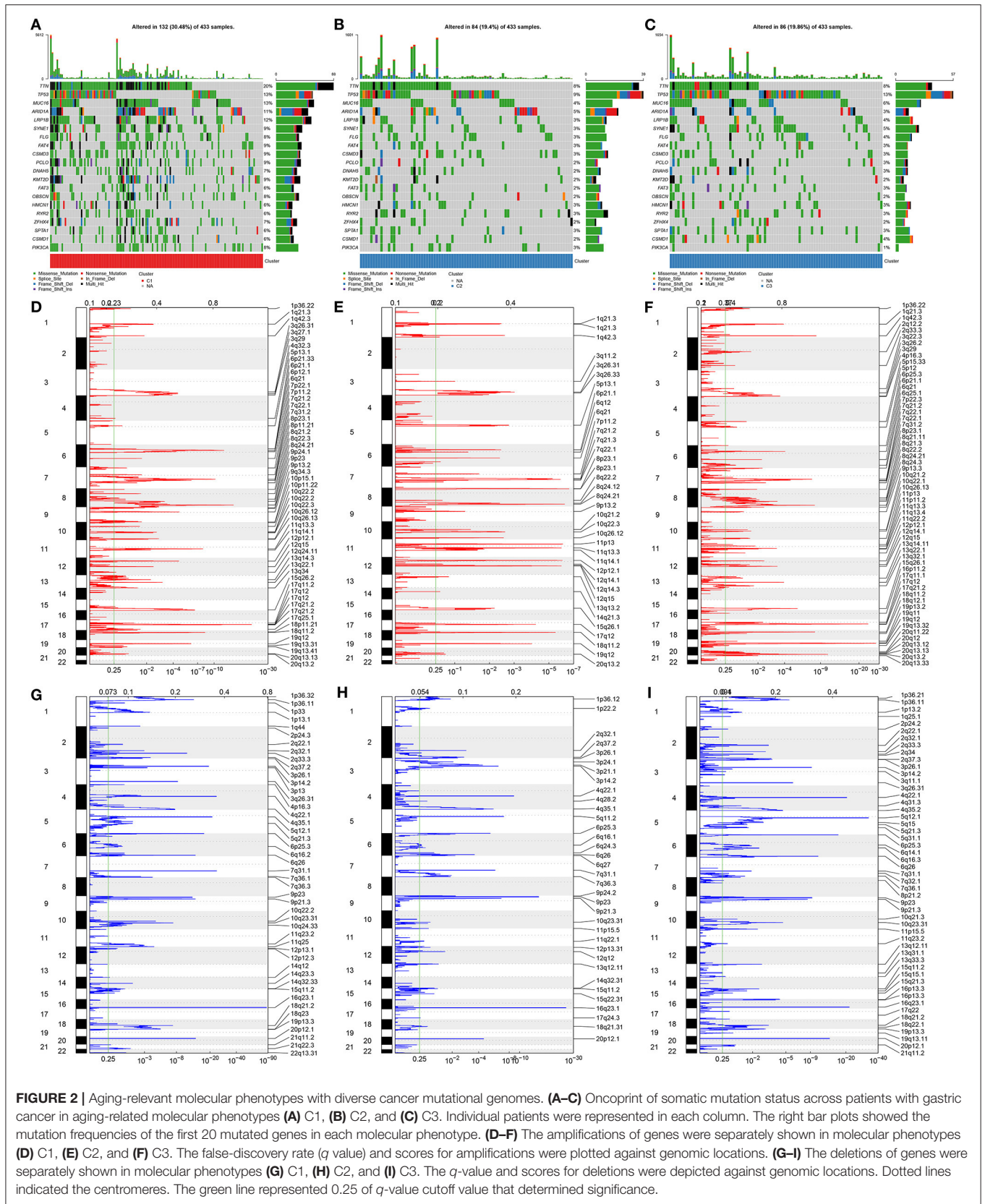
We further investigated the mechanisms underlying distinct aging-associated molecular phenotypes. In Figure 3A, we observed that immune activation pathways (complement, IL2-STAT5 signaling, inflammatory response, IL6-JAK-STAT3 signaling, allograft rejection, and interferon gamma response) and stromal activation pathways (epithelial-mesenchymal transition, angiogenesis, and WNT β -catenin signaling) were prominently upregulated in aging-associated molecular phenotype C2. Several tumorigenic pathways (mTORC1 signaling, MYC targets, DNA repair, E2F targets, and G2M checkpoint) presented a significant activation in molecular phenotypes C1 and C3. Consistently, pan-F-TBRS, immune checkpoint, EMT1-3, angiogenesis, and WNT target were prominently upregulated in molecular phenotype C2 (Figure 3B). The above data demonstrated the immune and stromal activation in molecular phenotype C2. The chemotherapeutic responses to sorafenib, gefitinib, vinorelbine, and gemcitabine were compared among three molecular phenotypes. Our results showed that molecular phenotype C2 presented the lowest therapeutic responses to sorafenib and gefitinib (Figures 3C,D) while phenotype C3 had the lowest therapeutic responses to vinorelbine and gemcitabine (Figures 3E,F).

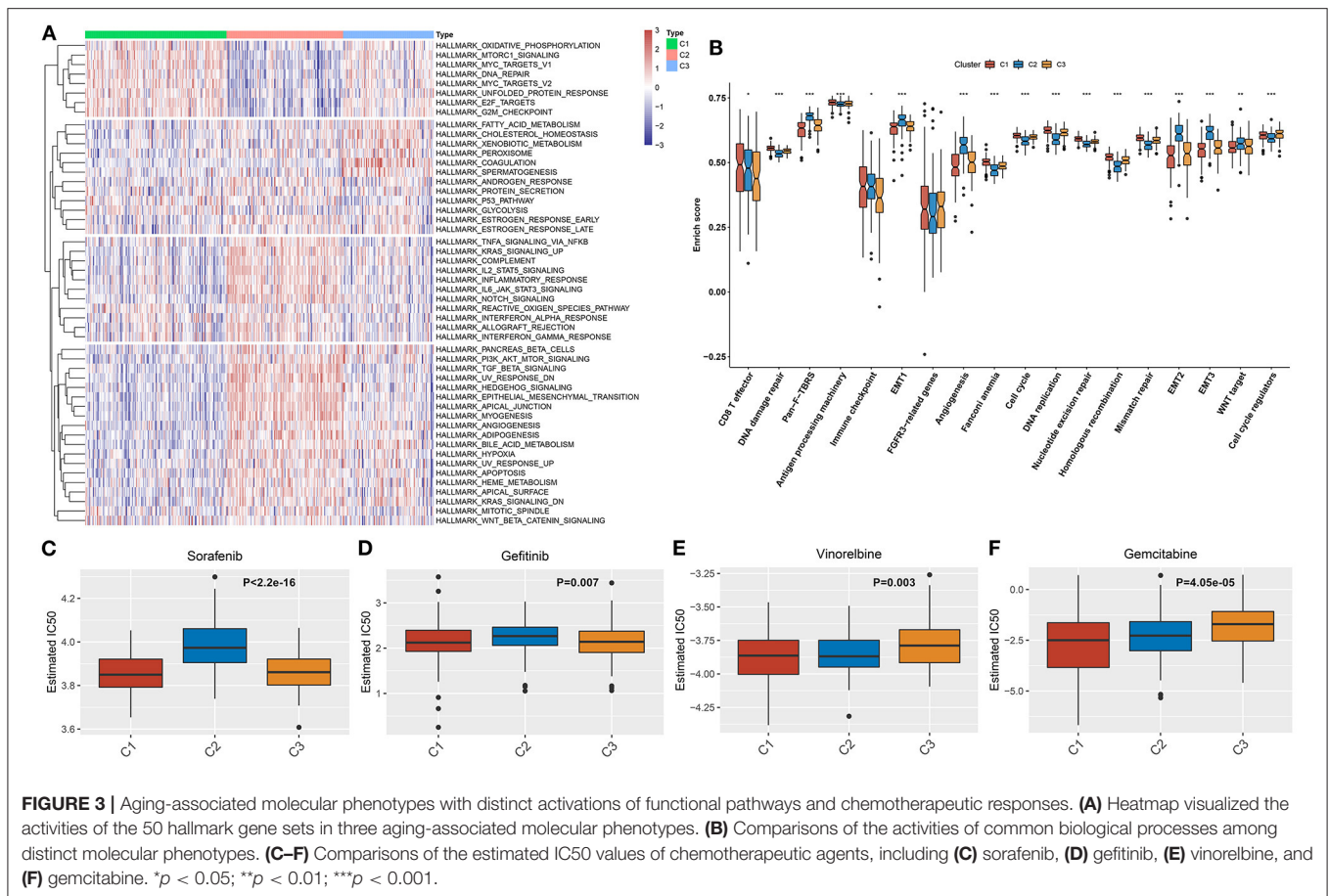


Aging-Associated Molecular Phenotypes Display Diverse Tumor Immune Microenvironment and Immunological Status

In **Figure 4A**, most MHC molecules (HLA-DMB, HLA-DOA, HLA-DOB, HLA-DPA1, HLA-DPB1, HLA-DQA1, HLA-DQB1,

HLA-DRA, HLA-DRB1, and HLA-E) presented the highest expressions in aging-associated molecular phenotype C2. This was indicative that the ability of antigen presentation and processing was upregulated in phenotype C2. Additionally, molecular phenotype C2 had the highest expressions of most chemokines (XCL2, CXCL1, CXCL12, CXCL13, CCL11, CCL13, CCL14, CCL16, CCL17, CCL19, CCL2, CCL21, CCL22, CCL23,



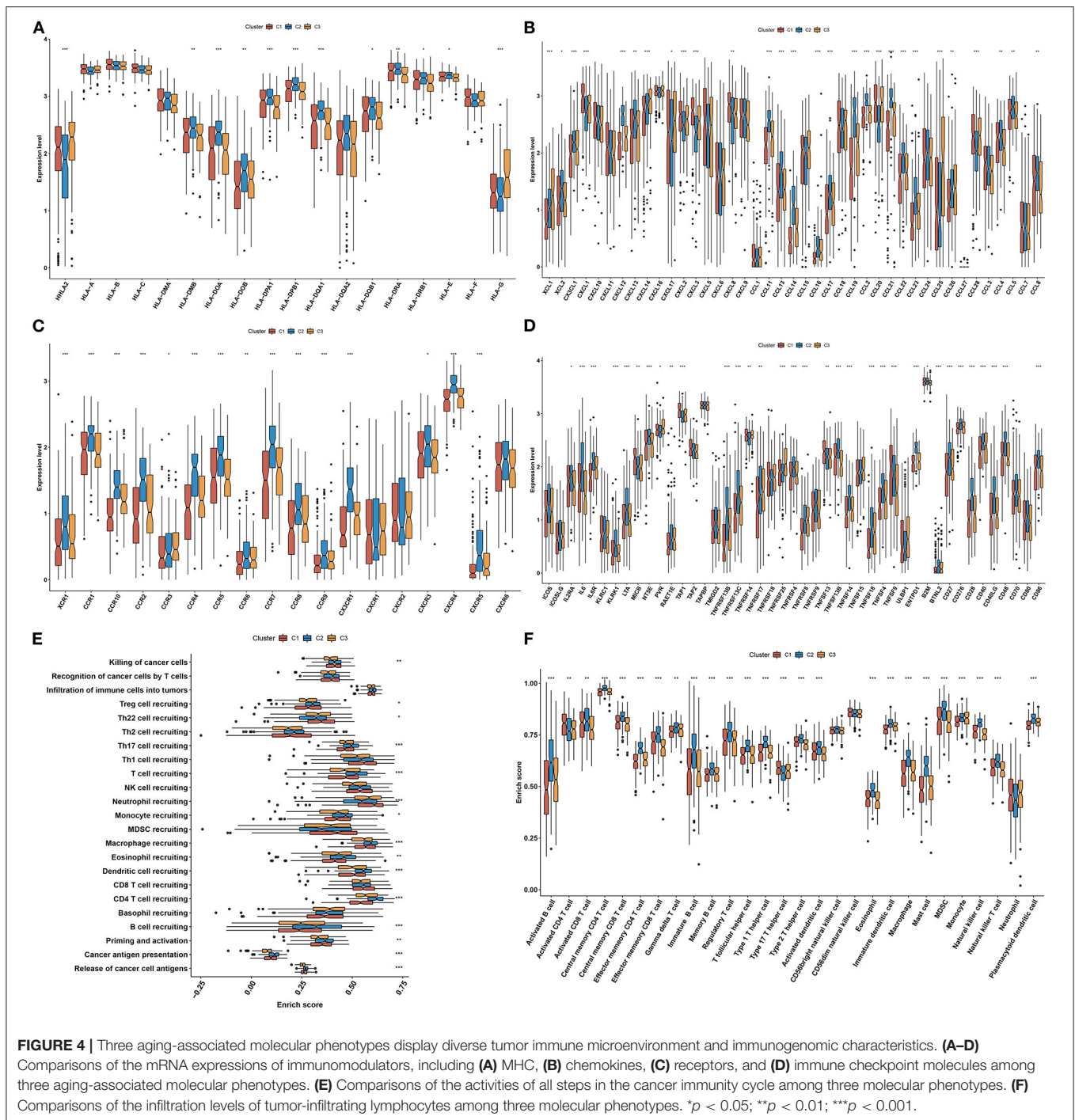


CCL4, and CCL8) and their receptors (XCR1, CCR1, CCR10, CCR2, CCR4, CCR5, CCR6, CCR7, CCR8, CCR9, CXCR1, CXCR3, CXCR4, and CXCR5), and the lowest expression of above molecules was found in molecular phenotype C1 (Figures 4B,C). Above chemokines and receptors facilitate the recruitment of effector lymphocytes like CD8+ T cell, TH17 cell, as well as antigen-presenting cells. In Figure 4D, molecular phenotype C2 was characterized by the highest expressions of most immune checkpoint molecules (IL2RA, IL6, IL6R, KLRK1, LTA, NT5E, RAET1E, TNFRSF13B, TNFRSF13C, TNFRSF17, TNFRSF4, TNFRSF8, TNFSF13B, TNFSF14, TNFSF18, TNFSF4, ENTPD1, BTNL2, CD27, CD276, CD28, CD40, CD40LG, CD48, and CD86). These data reflected the activated immunological status in molecular phenotype C2. Cancer immunity cycle activity is the overall manifestation of the chemokine system as well as immunomodulatory factors. Most steps in the cancer immunity cycle presented the highest activities in molecular phenotype C2, like cancer cell antigen release and presentation, priming and activation, recruitment of B cell, CD4 T cell, dendritic cell, eosinophil, macrophage, monocyte, T cell, Th17 cell, and Treg (Figure 4E). Thereafter, we calculated the infiltration levels of immune cells utilizing the ssGSEA algorithm. The infiltration levels of most immune cells were upregulated in molecular phenotype C2, like activated B cell, activated CD8 T cell, central memory CD4 T cell, central memory

CD8 T cell, effector memory CD4 T cell, effector memory CD8 T cell, gamma delta T cell, immature B cell, memory B cell, regulatory T cell, T follicular helper cell, type 1 T helper cell, type 2 T helper cell, activated dendritic cell, eosinophil, immature dendritic cell, macrophage, mast cell, MDSC, natural killer cell, natural killer T cell, and plasmacytoid dendritic cell (Figure 4F). Collectively, molecular phenotype C2 had an inflamed tumor microenvironment.

Aging-Associated Molecular Phenotypes Associated With Immunotherapeutic Response Predictors in Gastric Cancer

We investigated the difference in immunotherapeutic responses among three aging-associated molecular phenotypes through comparisons of multiple immunotherapeutic predictors. Aging-associated molecular phenotype C2 presented higher stromal and immune scores as well as reduced tumor purity compared with C1 and C3, indicating that samples in phenotype C2 had increased infiltrations of stromal and immune cells (Figures 5A–C). The mRNasi was quantified for reflecting the levels of cancer stem cells across gastric cancer. There was the lowest mRNasi in phenotype C2, while the highest mRNasi in phenotype C1 (Figure 5D). Also, we investigated the lowest SCNA in phenotype C2 but the highest SCNA in phenotype

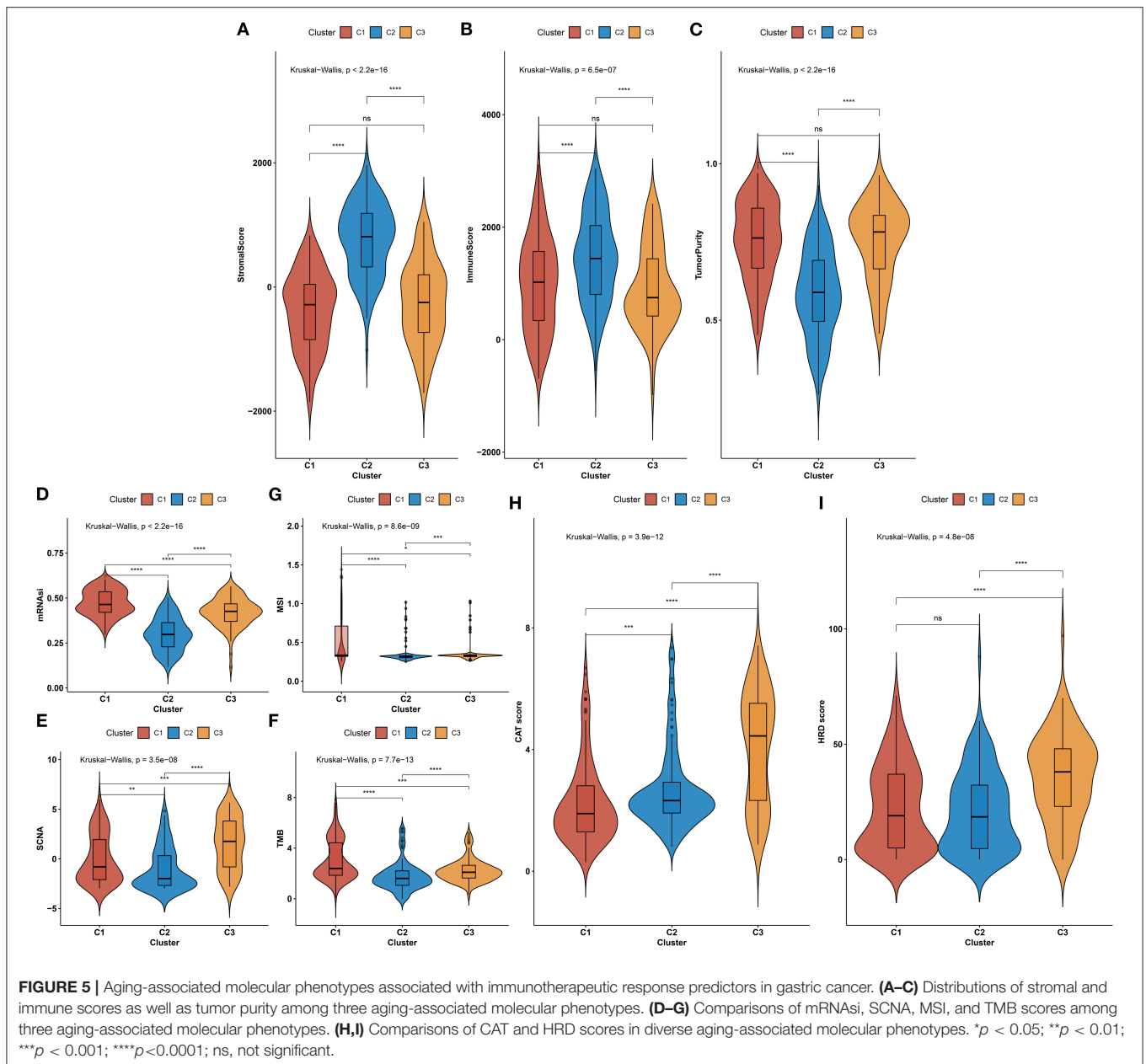


C3 (Figure 5E). In Figure 5F, phenotype C2 displayed the lowest MSI, while phenotype C1 possessed the highest MSI. Phenotype C2 presented the lowest TMB score but C1 had the highest TMB score (Figure 5G). We also evaluated the differences in cancer testis antigen (CAT) and HRD score among three aging-associated molecular phenotypes. We investigated that phenotype C3 had the highest CAT score, followed by C2 and C1 (Figure 5H). Additionally, the highest HRD score was

found in phenotype C3 (Figure 5I). The above data suggested that aging-associated molecular phenotypes presented distinct immunotherapeutic responses in gastric cancer.

Identification of Aging Molecular Phenotype-Relevant Key Genes

The WGCNA method was adopted for the construction of a co-expression network as well as finding genes highly



associated with aging molecular phenotypes. We first detected outliers among gastric cancer specimens on the basis of gene expression profiling. As a result, there was no outlier sample (**Figure 6A**). Thereafter, soft thresholding power β was calculated, and β was set at 5 for ensuring a scale-free network (**Figures 6B,C**). In total, 11 co-expression modules were merged, as depicted in **Figure 6D**. Among them, the brown module presented the strongest association with aging molecular phenotype C2 (**Figure 6E**). Thereafter, we evaluated intramodular analyses of genes in each module. Especially, genes in the brown module had high correlations with aging molecular phenotype C2 (**Figure 6F**). Eventually, 312 genes in this module were selected as aging molecular phenotype-relevant genes in

accordance with the criteria of module membership >0.8 and gene significance >0.5 (**Supplementary Table 3**). We further observed the interactions between aging molecular phenotype-relevant genes through the STRING database. With MCODE analyses, seven aging molecular phenotype-relevant hub genes were identified, namely, ACTA2, CALD1, LMOD1, MYH11, MYL9, MYLK, and TAGLN (**Figure 6G**). In **Figure 6H**, we noted that the hub genes displayed remarkable associations with the infiltration levels of immune cells. All of them were negatively correlated to the infiltration levels of activated CD4 T cell, CD56dim natural killer cell, neutrophil, and type 17 T helper cell but were positively associated with the other immune cells.

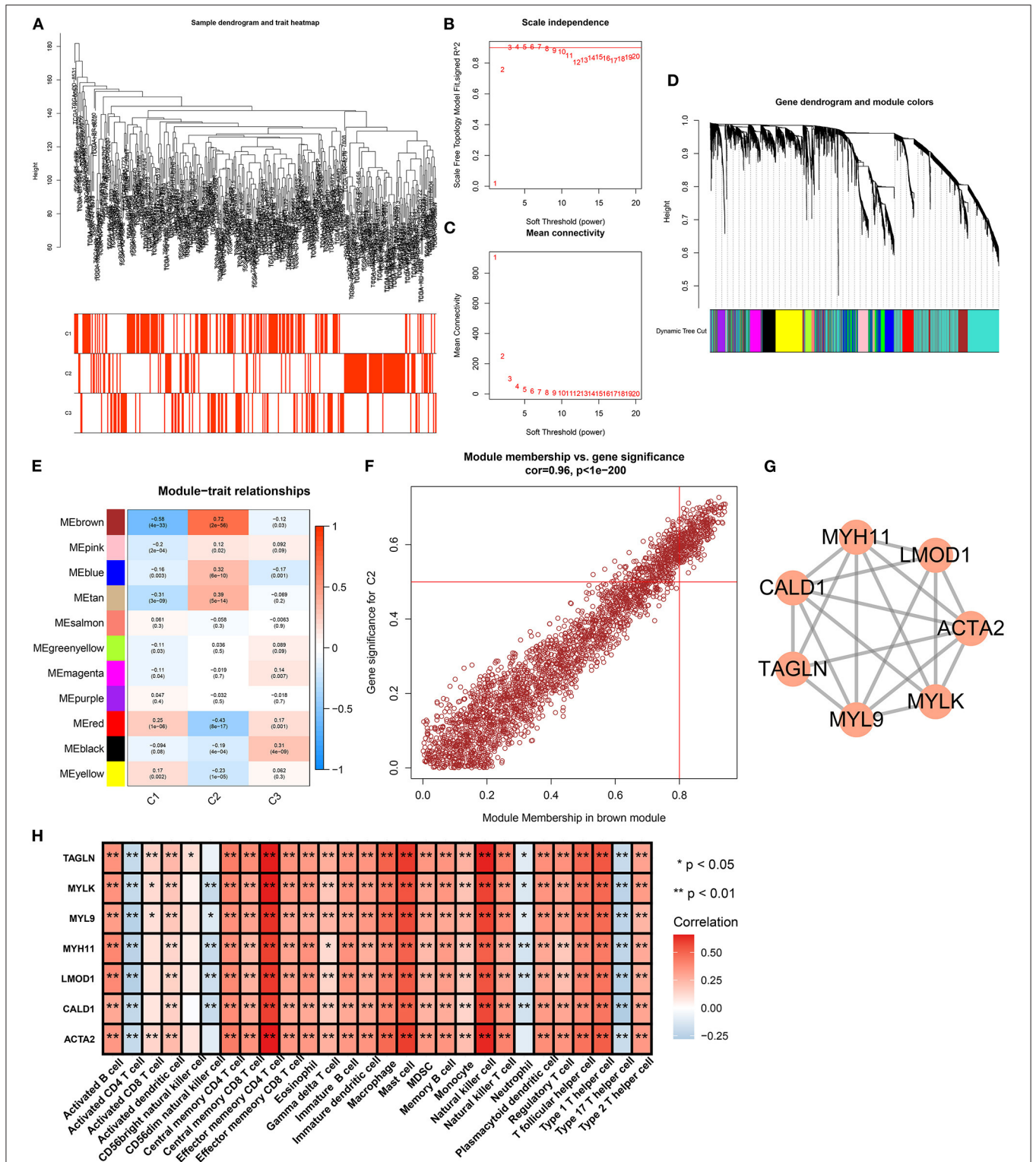
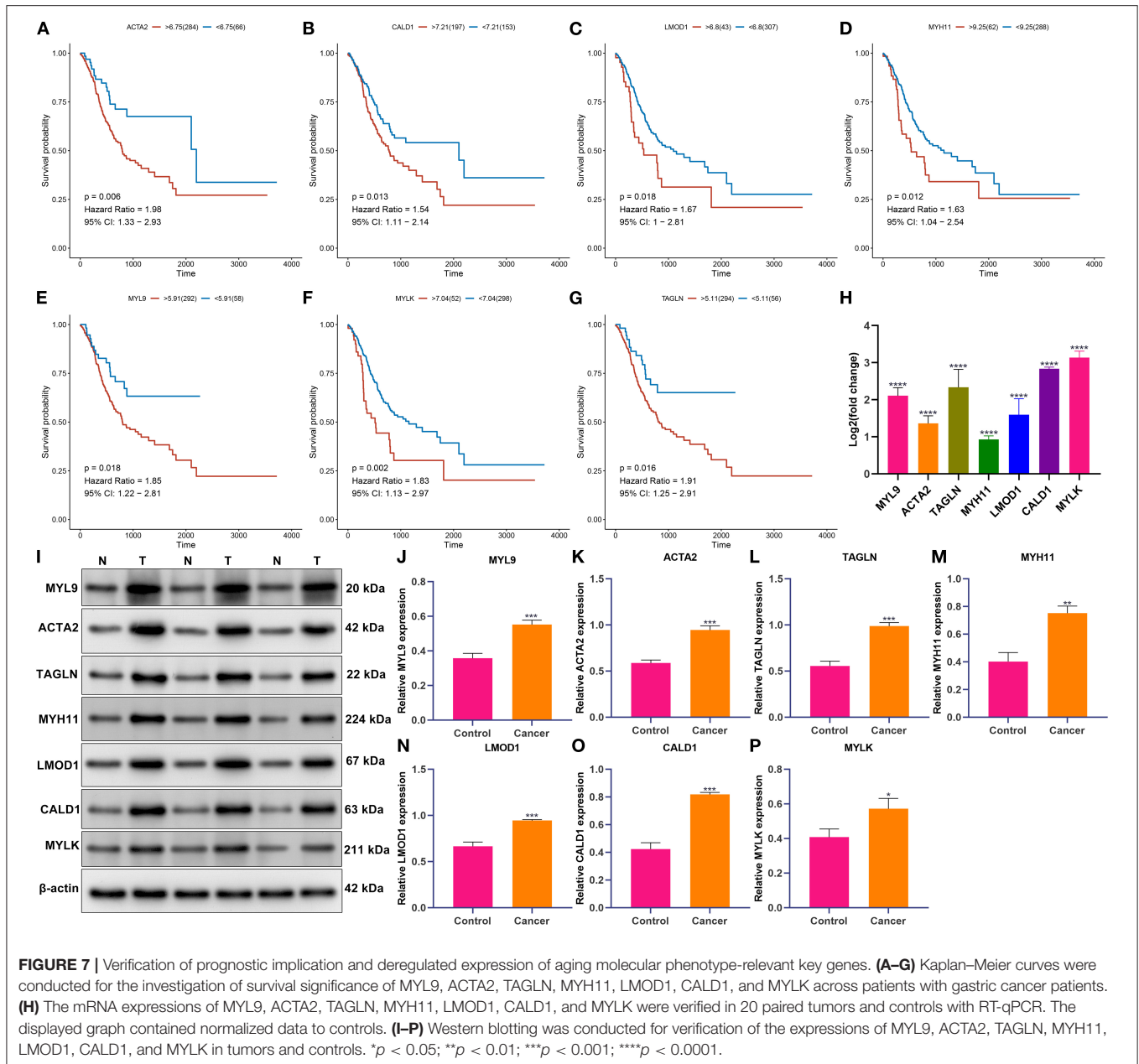


FIGURE 6 | Identification of aging molecular phenotype-relevant key genes. **(A)** Sample dendrogram and heatmap were conducted based on transcriptome data of gastric cancer. The color intensity indicated aging-associated molecular phenotypes (C1, C2, and C3). **(B)** The scale-free fitting index was determined across diverse soft thresholding powers. **(C)** Mean connectivity was analyzed under different soft thresholding powers. **(D)** Clustering dendrogram was conducted on the basis of co-expression network analyses. Totally, 11 co-expression modules were merged as well as uniquely identified by diverse colors. **(E)** Heatmap showed the correlation between co-expression modules and aging-associated molecular phenotypes across gastric cancer. The brown module presented the strongest correlation module with phenotype C2. **(F)** Scatter plots depicted the interactions of module membership in the brown module with gene significance for phenotype C2. **(G)** MCODE analyses identified the most prominent module in the PPI network of genes in the brown module. **(H)** Heatmap visualized the interaction between the hub genes and the infiltration levels of immune cells. * $p < 0.05$; ** $p < 0.01$.



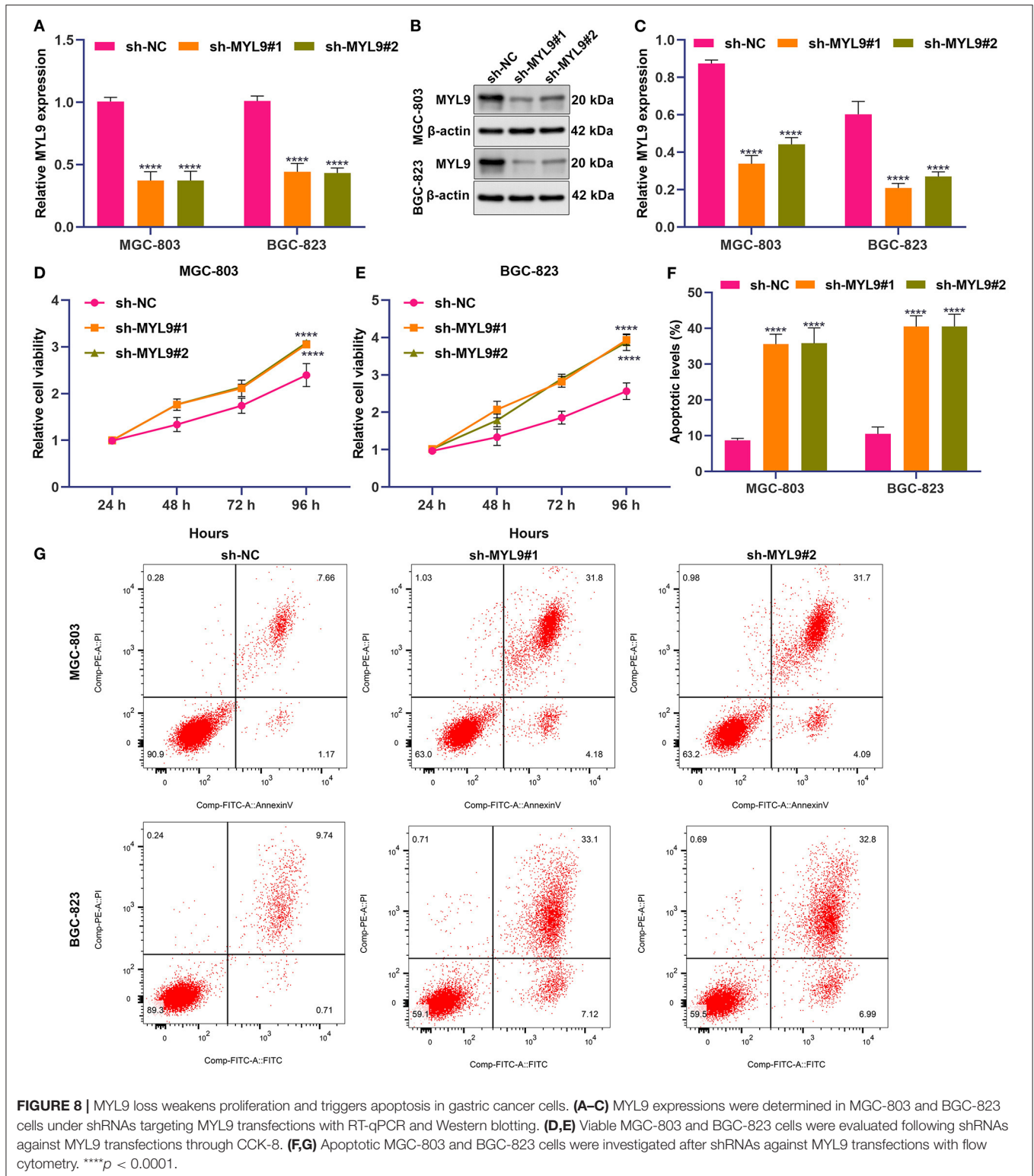
Verification of Prognostic Implication and Deregulated Expression of Aging Molecular Phenotype-Relevant Key Genes

Survival analyses were conducted for investigations of the prognostic implications of aging molecular phenotype-relevant key genes across patients with gastric cancer. Our data demonstrated that the upregulations of ACTA2, CALD1, LMOD1, MYH11, MYL9, MYLK, and TAGLN were in relation to more dismal survival outcomes in comparisons with their downregulations (Figures 7A–G). We further verified their expressions in 20 paired tumors and controls. In Figure 7H, compared with controls, their prominent

upregulations were investigated in tumors in line with RT-qPCR. Additionally, Western blotting results confirmed their abnormal expressions of these key genes in gastric cancer (Figures 7I–P).

In Gastric Cancer Cells, MYL9 Loss Weakens Proliferation and Triggers Apoptosis

Among aging molecular phenotype-relevant key genes, only the role of MYL9 in gastric cancer remains unknown. Thus, we investigated the function of MYL9 in gastric carcinogenesis. Herein, MYL9 expressions were reduced in



MGC-803 and BGC-823 cells under two shRNAs against MYL9 transfections (Figures 8A–C). In accordance with CCK-8 results, MYL9 loss reduced the cell viability of MGC-803 and BGC-823 cells (Figures 8D,E). Additionally,

apoptosis of MGC-803 and BGC-823 cells was enhanced when MYL9 expressions were defective (Figures 8F,G). The above data indicated the gastric tumorigenic roles of MYL9.

DISCUSSION

In our study, we conducted three aging-based molecular phenotypes with a consensus clustering algorithm. Further, aging-based molecular phenotypes were characterized by diverse clinical prognoses, mutational status as well as the immunological status of tumor microenvironment across gastric cancer. In this aspect, our findings offered individualized treatment options and prognosis evaluation for distinct subpopulations based on the aging-related molecular phenotypes.

The tumor microenvironment is comprised of a heterogeneous cellular milieu that influences cancer cell behaviors (3). The feature produces a far-reaching impact on treatment responses like immunotherapy. An inflamed tumor microenvironment combined with preexisting antitumor immunity is necessary for immunotherapy that suppresses tumor growth through tumor-cytotoxic T-cell re-invigoration. In theory, molecules and signals contribute to an inflamed tumor microenvironment that may trigger sensitivity to immunotherapy. Herein, in accordance with immunological features (immunomodulators, immune checkpoint molecules, cancer immunity cycle, and tumor-infiltrating immune cells), aging-based molecular phenotype C2 presented an inflamed tumor microenvironment. This indicated that the subpopulations in this phenotype possessed greater chances of responding to immunotherapy. Cancer stem cells contribute to chemotherapeutic resistance as well as distant metastases due to the self-renewal and tumorigenic capacities (37). Through mRNAsi, we quantified the levels of cancer stem cells across gastric cancer. There was the lowest mRNAsi in phenotype C2, while the highest mRNAsi in phenotype C1. TMB and MSI are capable of predicting the clinical responses to immunotherapy. Nevertheless, the predictors are examined utilizing complex molecular tools that are slow and expensive. Thus, it is an urgent medical requirement for developing faster and economical predictors. Our data indicated that phenotype C2 displayed the lowest MSI and TMB scores, while phenotype C1 possessed the highest MSI and TMB scores. HRD leads to impaired double-strand break repair, which is a common driving factor of carcinogenesis (38). Herein, phenotype C2 presented the features of reduced HRD score, while phenotype C3 was characterized by elevated HRD score.

Through WGCNA combined with MCODE methods, we identified seven aging molecular phenotype-relevant key genes, namely, ACTA2, CALD1, LMOD1, MYH11, MYL9, MYLK, and TAGLN. The above genes displayed the specific upregulations in gastric cancer and contributed to a dismal clinical prognosis. Previously, CALD1 acts as a prognostic indicator and also is in relation to immune infiltrates in gastric carcinoma (39). MYH11 expression is downregulated in gastric carcinoma and is indicative of a dismal clinical prognosis (40). Hypermethylation of MYLK serves as a circulating diagnostic marker of gastric carcinoma (41). Stromal fibroblasts in the microenvironment trigger gastric carcinoma metastases through the upregulation of TAGLN (42). Among them, our experimental pieces of evidence

demonstrated that MYL9 deficiency reduced proliferation as well as enhanced apoptosis in gastric carcinoma cells, confirming the tumorigenic function of MYL9. Nevertheless, there were a few limitations in this study. The aging-based molecular phenotypes should be further verified in large patients from multicenter cohorts for identifying the characteristics of clinical prognosis and drug responses. Additionally, we identified aging molecular phenotype-relevant key genes, especially MYL9. Nevertheless, the specific experimental verifications should be designed for the assessment of the biological implications.

CONCLUSION

Herein, our comprehensive assessment of the cellular, molecular, and genetic features correlated with aging-based molecular phenotypes generated novel insights on how gastric tumors responded to immunotherapy and guided the development of more effective combination therapeutic regimens.

DATA AVAILABILITY STATEMENT

The original contributions presented in the study are included in the article/**Supplementary Material**, further inquiries can be directed to the corresponding author/s.

ETHICS STATEMENT

The study was approved by the Ethics Committee of General Hospital of Ningxia Medical University (approval no. 2020-031). The patients/participants provided their written informed consent to participate in this study.

AUTHOR CONTRIBUTIONS

YZhu and SY conceived and designed the study. FH, HD, and YZhou conducted most of the experiments and data analysis and wrote the manuscript. YW and JX participated in collecting data and helped to draft the manuscript. All authors reviewed and approved the manuscript.

FUNDING

This work was funded by the National Key R&D Program of China (MOST-2017YFC0908300) and Ningxia Autonomous Region Key R&D Program Project (2018YBZD0418).

SUPPLEMENTARY MATERIAL

The Supplementary Material for this article can be found online at: <https://www.frontiersin.org/articles/10.3389/fmed.2021.792740/full#supplementary-material>

Supplementary Figure 1 | Validation of aging-genomic profiles identifies three molecular phenotypes across gastric cancer in the GSE84437 cohort. **(A)** Heatmap depicted sample clustering at consensus $k = 3$ following the transcriptome profiling of prognostic aging-relevant genes. **(B)** PCA plots

confirmed the classification accuracy of aging-relevant molecular phenotypes. **(C)** Heatmap showed the expression patterns of prognostic aging-relevant genes in three aging-relevant molecular phenotypes. **(D)** Kaplan–Meier survival curves were conducted for gastric cancer patients with diverse molecular phenotypes.

Supplementary Table 1 | Clinicopathological characteristics of patients with gastric cancer in TCGA and GSE84437 cohorts.

Supplementary Table 2 | The list of aging-relevant genes.

Supplementary Table 3 | The list of 312 genes in the brown module.

REFERENCES

- Gambardella V, Castillo J, Tarazona N, Gimeno-Valiente F, Martínez-Ciarpaglini C, Cabeza-Segura M, et al. The role of tumor-associated macrophages in gastric cancer development and their potential as a therapeutic target. *Cancer Treat Rev.* (2020) 86:102015. doi: 10.1016/j.ctrv.2020.102015
- Yan HHN, Siu HC, Law S, Ho SL, Yue SSK, Tsui WY, et al. A Comprehensive human gastric cancer organoid biobank captures tumor subtype heterogeneity and enables therapeutic screening. *Cell Stem Cell.* (2018) 23:882–97.e811. doi: 10.1016/j.stem.2018.09.016
- Sathe A, Grimes SM, Lau BT, Chen J, Suarez C, Huang RJ, et al. Single-cell genomic characterization reveals the cellular reprogramming of the gastric tumor microenvironment. *Clin Cancer Res.* (2020) 26:2640–53. doi: 10.1158/1078-0432.CCR-19-3231
- Ho SWT, Tan P. Dissection of gastric cancer heterogeneity for precision oncology. *Cancer Sci.* (2019) 110:3405–14. doi: 10.1111/cas.14191
- Zeng D, Li M, Zhou R, Zhang J, Sun H, Shi M, et al. Tumor microenvironment characterization in gastric cancer identifies prognostic and immunotherapeutically relevant gene signatures. *Cancer Immunol Res.* (2019) 7:737–50. doi: 10.1158/2326-6066.CIR-18-0436
- Yang J, Jiang Q, Liu L, Peng H, Wang Y, Li S, et al. Identification of prognostic aging-related genes associated with immunosuppression and inflammation in head and neck squamous cell carcinoma. *Aging (Albany NY).* (2020) 12:25778–804. doi: 10.18632/aging.104199
- Jia K, Cui C, Gao Y, Zhou Y, Cui Q. An analysis of aging-related genes derived from the Genotype-Tissue Expression project (GTEx). *Cell Death Discov.* (2018) 4:26. doi: 10.1038/s41420-018-0093-y
- de Magalhães JP, Costa J, Toussaint O. HAGR: the human ageing genomic resources. *Nucleic Acids Res.* (2005) 33:D537–543. doi: 10.1093/nar/gki017
- Avelar RA, Ortega JG, Tacutu R, Tyler EJ, Bennett D, Binetti P, et al. A multidimensional systems biology analysis of cellular senescence in aging and disease. *Genome Biol.* (2020) 21:91. doi: 10.1186/s13059-020-01990-9
- Serrano M, Lin AW, McCurrach ME, Beach D, Lowe SW. Oncogenic ras provokes premature cell senescence associated with accumulation of p53 and p16INK4a. *Cell.* (1997) 88:593–602. doi: 10.1016/S0092-8674(00)81902-9
- Labege RM, Zhou L, Sarantos MR, Rodier F, Freund A, de Keizer PL, et al. Glucocorticoids suppress selected components of the senescence-associated secretory phenotype. *Aging Cell.* (2012) 11:569–78. doi: 10.1111/j.1474-9726.2012.00818.x
- Faget DV, Ren Q, Stewart SA. Unmasking senescence: context-dependent effects of SASP in cancer. *Nat Rev Cancer.* (2019) 19:439–53. doi: 10.1038/s41568-019-0156-2
- Mahmoudi S, Xu L, Brunet A. Turning back time with emerging rejuvenation strategies. *Nat Cell Biol.* (2019) 21:32–43. doi: 10.1038/s41556-018-0206-0
- Johnson SC, Rabinovitch PS, Kaeberlein M. mTOR is a key modulator of ageing and age-related disease. *Nature.* (2013) 493:338–45. doi: 10.1038/nature11861
- Colaprico A, Silva TC, Olsen C, Garofano L, Cava C, Garolini D, et al. TCGAbiolinks: an R/Bioconductor package for integrative analysis of TCGA data. *Nucleic Acids Res.* (2016) 44:e71. doi: 10.1093/nar/gkv1507
- Yoon SJ, Park J, Shin Y, Choi Y, Park SW, Kang SG, et al. Deconvolution of diffuse gastric cancer and the suppression of CD34 on the BALB/c nude mice model. *BMC Cancer.* (2020) 20:314. doi: 10.1186/s12885-020-06814-4
- Liu Y, Sethi NS, Hinoue T, Schneider BG, Cherniack AD, Sanchez-Vega F, et al. Comparative molecular analysis of gastrointestinal adenocarcinomas. *Cancer Cell.* (2018) 33:721–735.e728. doi: 10.1016/j.ccell.2018.03.010
- Mayakonda A, Lin DC, Assenov Y, Plass C, Koeffler HP. Maftools: efficient and comprehensive analysis of somatic variants in cancer. *Genome Res.* (2018) 28:1747–56. doi: 10.1101/gr.239244.118
- Budczies J, Seidel A, Christopoulos P, Endris V, Kloor M, Gyorffy B, et al. Integrated analysis of the immunological and genetic status in and across cancer types: impact of mutational signatures beyond tumor mutational burden. *Oncotarget.* (2018) 7:e1526613. doi: 10.1080/2162402X.2018.1526613
- Mermel CH, Schumacher SE, Hill B, Meyerson ML, Beroukhi R, Getz G. GISTIC2.0 facilitates sensitive and confident localization of the targets of focal somatic copy-number alteration in human cancers. *Genome Biol.* (2011) 12:R41. doi: 10.1186/gb-2011-12-4-r41
- Davoli T, Uno H, Wooten EC, Elledge SJ. Tumor aneuploidy correlates with markers of immune evasion and with reduced response to immunotherapy. *Science.* (2017) 355:eaf8399. doi: 10.1126/science.aaf8399
- Wilkerson MD, Hayes DN. ConsensusClusterPlus: a class discovery tool with confidence assessments and item tracking. *Bioinformatics.* (2010) 26:1572–3. doi: 10.1093/bioinformatics/btq170
- Hänzelmann S, Castelo R, Guinney J. GSEA: gene set variation analysis for microarray and RNA-seq data. *BMC Bioinformatics.* (2013) 14:7. doi: 10.1186/1471-2105-14-7
- Liberzon A, Birger C, Thorvaldsdóttir H, Ghandi M, Mesirov JP, Tamayo P. The Molecular Signatures Database (MSigDB) hallmark gene set collection. *Cell Syst.* (2015) 1:417–25. doi: 10.1016/j.cels.2015.12.004
- Mariathasan S, Turley SJ, Nickles D, Castiglioni A, Yuen K, Wang Y, et al. TGF β attenuates tumour response to PD-L1 blockade by contributing to exclusion of T cells. *Nature.* (2018) 554:544–8. doi: 10.1038/nature25501
- Yang W, Soares J, Greninger P, Edelman EJ, Lightfoot H, Forbes S, et al. Genomics of Drug Sensitivity in Cancer (GDSC): a resource for therapeutic biomarker discovery in cancer cells. *Nucleic Acids Res.* (2013) 41:D955–961. doi: 10.1093/nar/gks1111
- Geeleher P, Cox N, Huang RS. pRRophetic: an R package for prediction of clinical chemotherapeutic response from tumor gene expression levels. *PLoS ONE.* (2014) 9:e107468. doi: 10.1371/journal.pone.0107468
- Sokolov A, Carlin DE, Paull EO, Baertsch R, Stuart JM. Pathway-based genomics prediction using generalized elastic net. *PLoS Comput Biol.* (2016) 12:e1004790. doi: 10.1371/journal.pcbi.1004790
- Auslander N, Zhang G, Lee JS, Frederick DT, Miao B, Moll T, et al. Robust prediction of response to immune checkpoint blockade therapy in metastatic melanoma. *Nat Med.* (2018) 24:1545–9. doi: 10.1038/s41591-018-0157-9
- Chen DS, Mellman I. Oncology meets immunology: the cancer-immunity cycle. *Immunity.* (2013) 39:1–10. doi: 10.1016/j.immuni.2013.07.012
- Yoshihara K, Shahmoradgoli M, Martínez E, Vegesna R, Kim H, Torres-García W, et al. Inferring tumour purity and stromal and immune cell admixture from expression data. *Nat Commun.* (2013) 4:2612. doi: 10.1038/ncomms3612
- Malta TM, Sokolov A, Gentles AJ, Burzykowski T, Poisson L, Weinstein JN, et al. Machine learning identifies stemness features associated with oncogenic dedifferentiation. *Cell.* (2018) 173:338–54.e315. doi: 10.1016/j.cell.2018.03.034
- Szklarczyk D, Gable AL, Nastou KC, Lyon D, Kirsch R, Pyysalo S, et al. The STRING database in 2021: customizable protein-protein networks, and functional characterization of user-uploaded gene/measurement sets. *Nucleic Acids Res.* (2021) 49:D605–12. doi: 10.1093/nar/gkab835
- Bader GD, Hogue CW. An automated method for finding molecular complexes in large protein interaction networks. *BMC Bioinformatics.* (2003) 4:2. doi: 10.1186/1471-2105-4-2
- Doncheva NT, Morris JH, Gorodkin J, Jøensen LJ. Cytoscape StringApp: network analysis and visualization of proteomics data. *J Proteome Res.* (2019) 18:623–32. doi: 10.1021/acs.jproteome.8b00702
- Zhang B, Wu Q, Li B, Wang D, Wang L, Zhou YL. m(6)A regulator-mediated methylation modification patterns and tumor microenvironment infiltration characterization in gastric cancer. *Mol Cancer.* (2020) 19:53. doi: 10.1186/s12943-020-01170-0

37. Sun L, Huang C, Zhu M, Guo S, Gao Q, Wang Q, et al. Gastric cancer mesenchymal stem cells regulate PD-L1-CTCF enhancing cancer stem cell-like properties and tumorigenesis. *Theranostics*. (2020) 10:11950–62. doi: 10.7150/thno.49717
38. Nguyen L, Materns, JWM, Van Hoeck A, Cuppen E. Pan-cancer landscape of homologous recombination deficiency. *Nat Commun*. (2020) 11:5584. doi: 10.1038/s41467-020-19406-4
39. Liu Y, Xie S, Zhu K, Guan X, Guo L, Lu R. CALD1 is a prognostic biomarker and correlated with immune infiltrates in gastric cancers. *Heliyon*. (2021) 7:e07257. doi: 10.1016/j.heliyon.2021.e07257
40. Wang J, Xu P, Hao Y, Yu T, Liu L, Song Y, et al. Interaction between DNMT3B and MYH11 via hypermethylation regulates gastric cancer progression. *BMC Cancer*. (2021) 21:914. doi: 10.1186/s12885-021-08653-3
41. Chen L, Su L, Li J, Zheng Y, Yu B, Yu Y, et al. Hypermethylated FAM5C and MYLK in serum as diagnosis and pre-warning markers for gastric cancer. *Dis Markers*. (2012) 32:195–202. doi: 10.1155/2012/473251
42. Yu B, Chen X, Li J, Qu Y, Su L, Peng Y, et al. Stromal fibroblasts in the microenvironment of gastric carcinomas promote tumor metastasis via upregulating TAGLN expression.

BMC Cell Biol. (2013) 14:17. doi: 10.1186/1471-2121-14-17

Conflict of Interest: The authors declare that the research was conducted in the absence of any commercial or financial relationships that could be construed as a potential conflict of interest.

Publisher's Note: All claims expressed in this article are solely those of the authors and do not necessarily represent those of their affiliated organizations, or those of the publisher, the editors and the reviewers. Any product that may be evaluated in this article, or claim that may be made by its manufacturer, is not guaranteed or endorsed by the publisher.

Copyright © 2022 He, Ding, Zhou, Wang, Xie, Yang and Zhu. This is an open-access article distributed under the terms of the Creative Commons Attribution License (CC BY). The use, distribution or reproduction in other forums is permitted, provided the original author(s) and the copyright owner(s) are credited and that the original publication in this journal is cited, in accordance with accepted academic practice. No use, distribution or reproduction is permitted which does not comply with these terms.